IIETA International Information and Engineering Technology Association
Advancing the World of Information and Engineering

Traitement du Signal
Vol. 39, No. 1, February, 2022, pp. 239-246
Journal homepage: http://iieta.org/journals/ts

A Rapid Advancing Image Segmentation Approach in Dental to Predict Cryst

Prasath Sivasankaran[1*], Karthigarani Dhanaraj[2]

[1] Department of Computer Science, VET Institute of Arts and Science (Co-edu) College, Erode 638012, Tamil Nadu, India
[2] Department of Computer Science, Nandha Arts and Science College, Erode 638052, Tamil Nadu, India

Corresponding Author Email: prasaths@vetias.ac.in

https://doi.org/10.18280/ts.390124

Received: 16 December 2021
Accepted: 12 February 2022

Keywords:
CAD, X-ray images, maximal IsoCenters, Fastly marching methodology, image processing, detection of dentistry cysts, radiologists

ABSTRACT

A teeth X-rays image exhibits low intensity & irregular illumination, resulting in loss of solid distinction among distinct sections of the tooth, making tumor separation time-consuming. That isophote curvature is the line that connects pixels of the same brightness. Every isocenters is related to every isophotes curvature line. That Maximal IsoCenters (MIC) serves as the starting point for the rapid marches technique's model-based segmented. Its Fastly Marching Methodology (FMM) was similar to Dijkstra's algorithms in that it takes the quickest route from of the promoter regions, wherein data simply travels outwards. It operates in a methodical way to speed things up, and that's a one-pass approach although each spot is mostly just handled once. As a result, combining prototypes with the feature-based categorization of dentistry X-rays images offers a lot of promise in terms of diagnosing tooth disorders & helping to design electronic machines. This segmentation and classification technique computerizes or automates the testing process, allowing for the monitoring of a significant number of patients with much the same exactness. Rising machines aid in the production of fast and effective outcomes. Computer's systems make it feasible to expand patient safety to far places by allowing for speedier interaction.

1. INTRODUCTION

This automating of computers-aided diagnostic diagnostics in a vast dataset makes digitized dentistry X-rays analysis more extremely simple in the area of dentists [1]. A tooth cyst is a serious issue that produces severe discomfort in the afflicted area, spreading to the jaws, cheeks, & head. As a result, it's critical to eliminate the cysts to prevent the disease from spreading to other regions of the oral [2]. Computers-aided identification/diagnostics (CAD) have suddenly been a popular topic of study in digitized tooth X-rays. Computer-assisted diagnostics improve diagnostic performance, measures harshness, detect tooth cysts automatically, and speed up the human driver's viewing & comprehension of medical images [3]. Dentistry diagnostics would be aided by the adoption of CAD-based digitized oral X-rays since dental professionals can detect the concealed bones & teeth beneath the surface of the cortical plate throughout site observation. The key benefits of dentistry X-ray images are their immediate accessibility, low radiations dosage, capacity to improve and rebuild images, including the use of CAD to enable oral X-rays analysis easier accessible [4].

Improved diagnostic, as well as judgment for the dentist's subsequent treatments method, has grown simpler with the emergence of computer-aided diagnostics/detecting [5]. Radiologists rely on computer-assisted procedures to make keeping accurate diagnoses. There isn't a single automatic image segmentation approach that works for all types of photographs. Based on the applications domain, image separation must be distinctive and much more sophisticated [6]. Overall panoramic views, periapical view, as well as bitewing perspective are the 3 levels available on computerized dentistry X-rays. This periapical image, which contains merely a few teeth plus associated roots as well as bones in the nearby region, is one of the most commonly utilized. Such periapicals images are in handy for detecting disorders such as bones losses incurred by periodontal disease & tooth cavities [7]. Regular intervals oral X-rays are by far the most extensively utilized modalities in dentistry photography, but making them entirely automated for computer-aided diagnosis and monitoring of tooth illnesses is a difficult task.

2. MATERIALS AND METHODS

Manually, semi-automatic, & automated segments are the three types of medical image segments. Manually segmented explains the technique in which a medical specialist segment as well as classifies a clinical image by hands, depending on that categorization [8, 9]. The term "automated segmented" refers to a procedure in which the software assigns section borders mechanically. Semi-automated categorization refers to the procedure in which automatic segmentation is accompanied by human assessment as well as the divided borders are determined. There are 3 kinds of separation in cysts delineation. This livewire method by Meerbeek et al. [10] is used here for manual segmentations. The expanding the using digitized diagnostic radiology & CBCT scanning for dentistry detection, therapeutic, including medical investigations necessitates the use of computers to assist radiologists in diseases diagnosis plus treatments [11]. Again for identification of the Regions of Interests (RoI), dependable and reliable techniques are in short supply.

Levels set technique, livewire, and dynamic contours are the most common semi-automatic approaches. Deformable models, which are prototype strategies for area boundaries demarcation, encompass all semi-automatic techniques [12]. These employ materials or enclosed shapes which change when subjected to internal or external stimuli. A surface or enclosed curved would be placed closer to the intended entity border to delineate the entity boundaries. It would then be permitted to go into an incremental relaxing procedure [13]. Key benefits of this deformation system would be that it can build surfaced or closed curved from desirable images with the addition of a smoothness parameter restriction, which provides resilience to noisy & erroneous borders. The downside of this technique would be that it needs manual intervention for the first modeling placement & parameter estimation [14].

Some development of autonomous categorization includes the ability to computerize or automate the clinical diagnosis to monitor a lot of patients with much the same level of certainty. Machines with strong computing speeds aid in obtaining quick and accurate answers [15]. Computers networks make it feasible to expand patients' safety to far places by allowing for speedier communications. Prototype levels setting technique, similarity-based sector growth strategy, histograms based cutoff approach, masks based patterns matching, and textures based segmented are among the completely automatically approaches previously presented for identification of lesions in dentistry X-rays, according to the survey. Miracle et al. [16] presented a particles swarm optimizations & adaptively threshold approach for segmenting hepatic tumors. Polonsky et al. [17] suggested MSER-based classification for hepatic tumor delineation.

Human inspections provide only subjective data that varies from dentists to dentists that do not provide quantitative datasets [18]. Simultaneously, even some initial tumors would be invisible to the naked eyes. Conventional segmentation techniques have a higher probability of wrongful convictions and are more susceptible to segmented mistakes. Every one of the issues listed above demonstrates the challenges of applying automation categorization in computer-aided diagnostics, as well as the need for highly precise and effective automated dentistry X-rays interpretation [19, 20]. The results of a literature search for tooth X-rays lesion segmentations. It included information on the modalities, viewpoint, and forms of carious lesions, cysts, as well as plaques, as well as segmentation approaches such as semi-automatic & completely automated. The majority of the procedures were automated, reducing the need for human involvement. This suggested two-stage, completely automated hybrids technique combining Isophotes curvature and rapid advancing algorithms would solve the problems in cysts identification discussed previously [21]. The suggested approach for cyst border identification is new rapid, hybrids, as well as two-stages automated segmentation methods.

2.1 Modeling studies on the dental cyst

This tumor is a capsule that forms in the tooth roots and induces infections by causing nerve roots irritation in the tooth membranes. A dentistry tumor is a serious issue that produces abrupt discomfort in the afflicted area before spreading to the jaws, cheeks, & forehead.

As a result, it's critical to eliminate the tumor as well as prevent infections from spreading to other regions of the tongue [22]. These nerve root &follicular cysts, which are generally cylindrical & illustrated in Figure 1, are categorized as radicular and follicular cysts depending on numerous parameters such as position, etiology, & form.

A picture's isophotes resemble topographic maps, which are lines traced thru a consistent region of intensity. This is the most important geometrics information in a image since it provides the relationship of surfaces spots with consistent brightness & sharpness via curves known as isophotes or leveling lines. Both core & lining of the tumor become the more obvious round characteristics of the tumor when compared to the isophotes feature. Along the lumens as well as lining, these have such a continuous grey value. That brightness would be roughly the same inside the tiers. As a result, this should define the characteristics of cysts utilizing isophotes, which are curves linking locations of equal intensities that do not meet. As a result, isophotes denotes a character that has the same grey value in the cystic region's round or semi-circular regions.

A hybrids technique for locating the eyes in low-resolution photographs was presented [23]. Experts classified the eyeball based on its structure, which is distributed over the entire in luminance. As a result, they constitute the core of round or semi-circular designs with isophotes. Adjustments in longitudinal illumination as well as in rotations do not affect the isophotes. Tumors contained bilaterally symmetrical light patterns, just like the eyes. Its follicular and radicular cysts are usually round or semi-circular in shape. As a result, scientists may use isophotes to determine the luminance of bilaterally symmetrical round & semi-circular designs [24]. Follicular cysts have a circularity of 0.807 ± 0.149 & radiculars tumors have a circularity of 0.932 ± 0.086. which has been observed as well as presented.

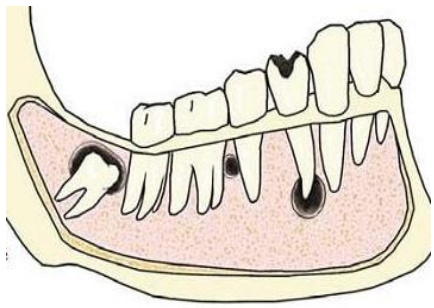

Figure 1. Dental cyst

3. PROPOSED METHOD

When separating the oral tumor from the periapical X-rays image, many images segmentation algorithms were used. Prototype segmented, features-based categorization, & hybrid approaches are the three types of fragmentation. Some benefits of prototype approaches include particularly resilient as well as exact in inspection to using the worldwide presentation, however, the outcome is solely dependent on the model's agreement [25].

Dynamic shapes and appearances models, dynamic contouring plus flexible templating, including levels-set oriented approach are among the previous knowledge-based segmentation techniques. Features-based approaches, on the other hand, use distinguishing traits (such as symmetrical) to recognize objects from localized image characteristics (e.g., borders, sides, and slopes) without the need for a learnings

approach or model fitting. Even in a loud environment, features-based approaches may quickly detect the objects. It is, nevertheless, possible that it is erroneous & much less reliable than prototype solutions. Image segmentations vary based on applications, format, bodily area, as well as other factors. No one segmentations process could deliver accurate, appropriate, as well as automatic outcomes. The overall efficiency of segmented may be improved by integrating several segmentations algorithms to create a hybrids architecture. As a result in Figure 2, it can improve outputs performance while reducing the weaknesses of particular techniques. Prototype rapid protesting plus features-based isophotes approaches are coupled in the suggested methodologies to provide excellent performance as well as make it entirely automation in minimizing manual demarcation by human operators in a big medical record.

The very first-degree gauging frames in the image is the localized pairing of units dimensions v, w, whereby v endpoints are already in isophotes tangentially directions and w endpoints will be in the gradient directions, that is perpendicular to v. As a result, each pixel in a photo that is tied to the t, u locals frame, that is aligned differentially including gradients of t&u. ∂M ∂u = Mi and ∂M ∂t ≡ 0 is resistant to translational and rotational when the magnitude of the gradient is equal inside the tangential directions of isophotes, there are no brightness changes. Where ∂M, ∂t, ∂u represents change of length, displacement in direction and directional derivation respectively [26].

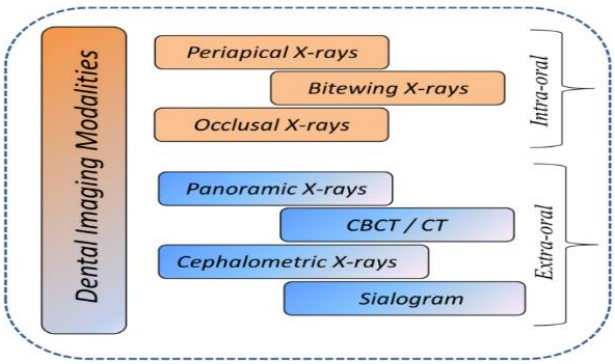

Figure 2. Dental cyst model

$$u^{\wedge}=\{M_i, M_j\}/\sqrt{M_i, M_j};\ t^{\wedge}=\lrcorner u^{\wedge} \quad (1)$$

$$u=1/\sqrt{M_i, M_j}\begin{pmatrix}Mi\\Mj\end{pmatrix},\ t=\begin{pmatrix}0 & 1\\-1 & 0\end{pmatrix}*u \quad (2)$$

Definition of isophotes was M(u, t(u)) = constants & differentiating isophotes definitions concerning,

$$M_u+M_t t'(u)=0;\ t'(u)=-M_u/M_t \quad (3)$$

Condition of gauge Mu=0 tends to t'(u)=0. From isophotes definition we get

$$M_{uu}+2M_{ut}t'(u)+M_{tt}t'(u)^2+M_t t''(u)=0 \quad (4)$$

Isophote curvature can be

$$L=-M_{uu}/M_t \quad (5)$$

Isophote curvature can be defined as t''(u), the modification of tangent vector t' (u) in u direction.

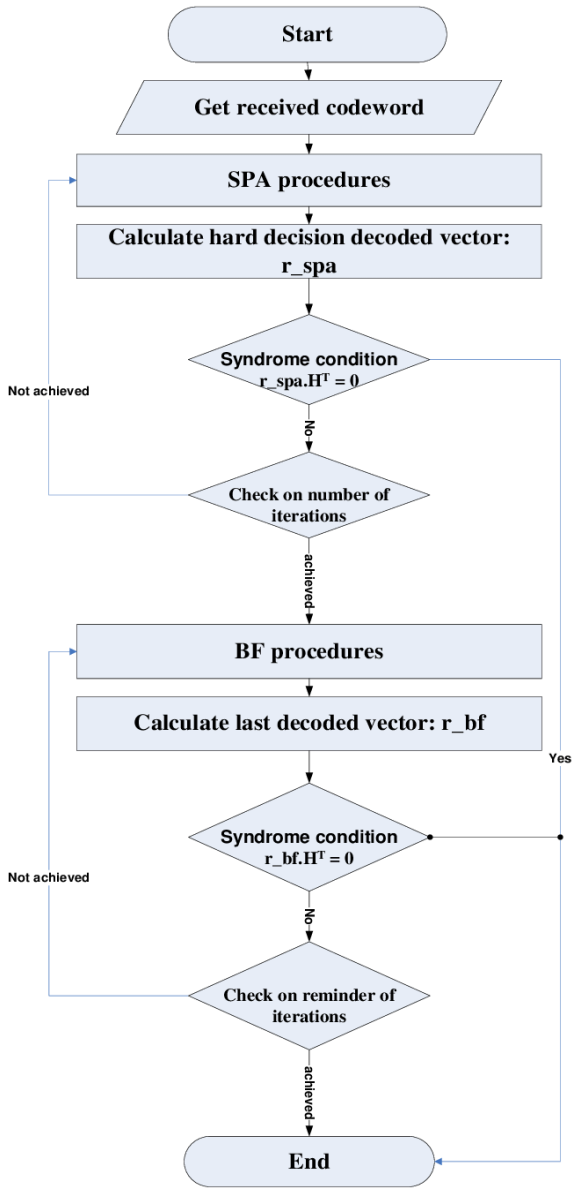

Figure 3. Process flow for the proposed technique

$$L=-M_{uu}/M_t=-M_j^2M_{ii}-2M_iM_{ij}M_j+M_i^2M_{ij}/\sqrt{M_i^2M_j^2} \quad (6)$$

Mi, Mj is the first-order derivatives and second layer derivatives are Mij, Mii, Mjj.

The lower-order variants computed in Table 1.

The reciprocal of the curvature is given by

$$S=(L)^{-1}=-(M_j^2M_{ii}-2M_i\,M_{ij}M_j+M_i^2M_{ij}/\sqrt{M_i^2M_j^2})^{-1} \quad (7)$$

Because the gradients are needed to calculate the inclination [27], This bending signature is determined by the curves outside intensities values. Because the cysts' exterior border is clearer, the indication of bending is favorable. A combination of the inversion of isophotes curvature with the gradients {Mi, Mj}/Mt yields the displaced vectors. These displaced indices Ei and Ej correspond to the model generated by the centers.

$$\{E_i,E_j\}=\{M_i,M_j\}/M_t(-M_t/M_{uu})=-\{M_i,M_j\}/M_{uu} \quad (8)$$

$$\{E_i,E_j\}=\{M_i,M_j\}(M_i^2,M_j^2)/M_i^2M_{ii}+2M_iM_{ij}M_j+M_i^2M_{jj} \quad (9)$$

This collection of indicators is pointed towards the circular structure's center. This integrator is an approximate estimate

of the center based on the collectives voting of the displaced variables. This Gaussian kernel is combined with both the accumulation because it is an approximate approximation of the center in Figure 3.

Table 1. Differential formulation for low order

M_u	0
M_t	$\sqrt{M_i^2 M_j^2}$
M_{uu}	$-M_j^2 M_{ii}-2M_i M_{ij} M_j+M_i^2 M_{ij}/M_i^2 M_j^2$
M_u	$\{M_i,M_j\}(M_i^2,M_j^2)M_i^2 M_{ii}+2M_i M_{ij} M_j+M_i^2 M_{ji}/M_i^2+M_j^2$
M_{tt}	$-M_j^2 M_{ii}-2M_i M_{ij} M_j+M_i^2 M_{ij}/M_i^2+M_j^2$

That's an imaging operator for calculating the divergence of an area's smoothness as well as how bent it is. The curvedness attribute determines whether twisted the form is. Its curvedness is a rotational invariants gradient operator that gauges the gradient's acceleration.

$$\text{Curvedness}=\sqrt{Mii^2+2Mij^2+Mjj^2} \quad (10)$$

Over flat roofs as well as objects surfaces, that metric has a smaller response. It responds more strongly in areas with the highest isophotes density, such as along the entity's borders. The concentration of the isophotes is directly related to the curvedness. Isophotes have a stronger reaction, indicating that both share a comparable characteristic, such as an edge, and are oriented in the same direction [28]. Isophotes that are thicker have a stronger curvedness. The only isophotes that are regarded have high curvedness, which is generally seen at an entity's border. Another benefit of weighting center votes by curvedness across an edge-based technique is that it prevents useless isophotes surrounding borders. Isocenters, or ICs, refer to the stronger reactions. The maximal accountable isocenters are determined to be the best practicable estimation for determining the tumor area between individuals.

Round or semi-circular tumor lumens, as well as surrounding cells, are very well. Inside the stages, every pixel's brightness would be about the same. With this background, the suggested technology employs the most accountable isocenters as seeding in the cavernous region. That form of the lumens & linings is used to locate the site of the seeds and thus are referred to as Isophotes curves. Applying Eqns. (1-5) order variations were computed to get the Isophotes curvatures (6). Utilizing Eqns. (7, 8), mix the image gradients with both the inversion of the Isophotes curvature to find the movement vectors (9). This curvedness, which itself is determined by Eq. (10) to identify the cysts isocenters and encoded just on accumulators, gives each pixel a distinct weighting. That metric of curvedness is used to find significant isocenters in the cystic area [29]. That MIC is utilized as the starting points or seeding points for the FMM to partition the tumor amongst on isocenters. This procedure is illustrated in Figure 4 as a diagram showing intermediary findings.

3.1 Cyst segmentation using fast marching method

Regarding oral tumor removal, a prototype technique called the FMM is applied. Figure 4 depicts the many processes required in tumor removal, with a comprehensive explanation provided below. Very fastly marching equations is a numerical method created by Sethian (1996) for addressing boundaries value issues of Eikonal Eq. (11).

$$G(i).|\Delta U(i)|=1 \quad (11)$$

That numerical approach solves the problems of curved evolutions in a sealed curved having time U&G(i) velocity in the normal directions on a curved at points i. Getting the right answer to the equations provides the speed, time at which the contours approach points i. This method is related to Dijkstra's algorithms, but it starts at the seeds point & continues the route. As a result, knowledge only travels outwards. Furthermore, levels setting approaches are a subclass of this technique. These levels setting approach is, in general, quite sluggish. For all duration, the border is constructed to signify the development or contracting of the boundaries value issue. Letting the interfaces move in one plane produces an efficient, rapid marchings strategy. That interaction is termed fringes following if it propagates to the next nearest integer until something approaches the unidentified nodes closest to the knowing nodes. Another viscoelastic solution to the previously mentioned Eikonal Eq. (12) is provided by

$$|\Delta v(i)|=G(i) \quad (12)$$

These envelopes of the fresher frontal develop additional points, as well as the process is repeated until the Eikonal solutions are obtained. This fundamental concept is to solve the problem precisely by beginning with the known regions. In the area indicated in Figure 5, the front is also gradually moving within the curves or surfaces from the boundaries.

As for multi-dimensional boundaries values formulation

$$|\Delta v(I,j,k)|=f(i,j,k) \quad (13)$$

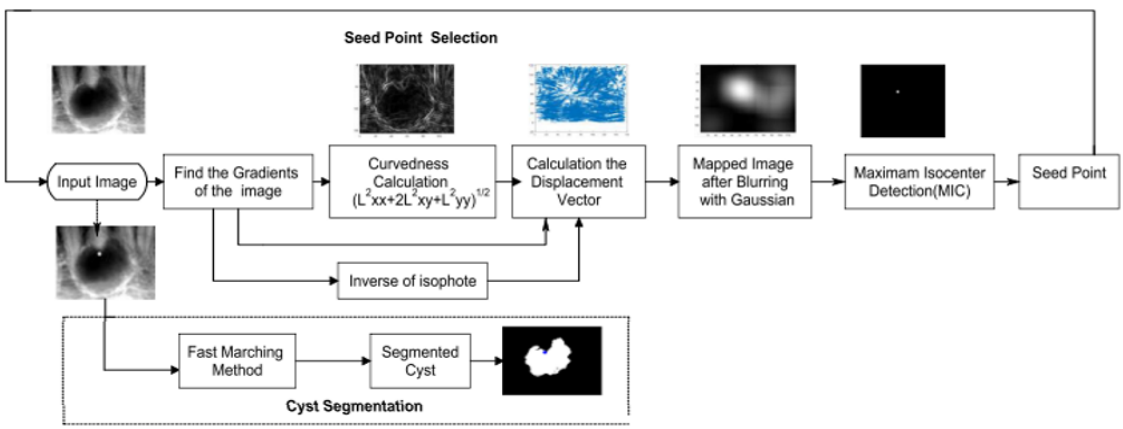

Figure 4. Hybrid approach

Approximates of multi dimension

$$|\Delta v|=[\sum_{u=i,j,k}(\mathrm{Max}(\mathrm{Eijk}\,v,0)+\mathrm{Min}(\mathrm{Eijk}\,v,0)_n)]=g_{ijk} \quad (14)$$

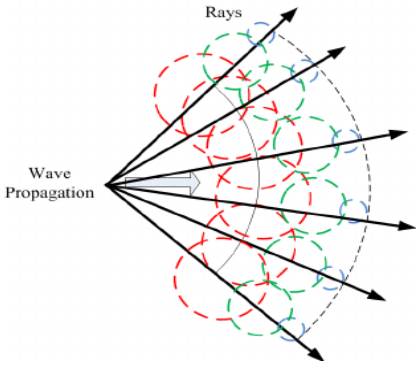

Figure 5. Front propagation rays

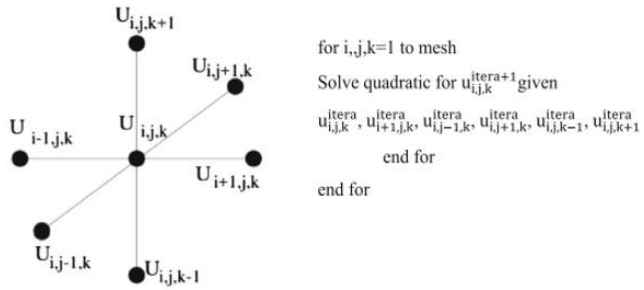

Figure 6. Updating the grid points

$$\begin{bmatrix}\mathrm{Max}\left(E_{ijk_n}^{-i}v-E_{ijk_n}^{+i}v,0\right)^2+\\ \mathrm{Max}\left(E_{ijk_n}^{-j}v-E_{ijk_n}^{+j}v,0\right)^2+\\ \mathrm{Max}\left(E_{ijk_n}^{-k}v-E_{ijk_n}^{+k}v,0\right)^2+\end{bmatrix}=g_{ijk} \quad (15)$$

where, in forwards as well as backward are the same forwards as well as backward operators, E-and E+ seem to be the same forwards and backward operators. There at grids point ijk depicted in Figure 6, Eiji is sluggish.

3.2 FMM algorithm

On such networking, this rapid marches approach connects using shortest paths algorithms, also known as Dijkstra's technique. Dijkstra's approach is a well-known routable technique. An Eikonal is originally a group of points known as Approved spots. It is also the computed experimental solutions to Eq. (15) for the given values of 'u,' to obtain the acceptable neighbor for each point sin the grids that have not yet been approved. Next, inside the starting conditions mark all of the items as 'Acknowledged.' Now, by calculating Eq. (15), the spots that are one grid point away were labeled as 'Regarded,' and all other locations are classified as 'Far.'

This is a very excellent method for sorting the route in which the nearby locations' costs are taken into account. It operates in a methodical way to speed things up, and that's a one-pass approach because each point is only touched once. The key to this methodology is the quick process of selecting the grid points in the narrow bands with the minimum u number. This fastly marching method's computational performance for meshes with N nodes is O. (N log N). This efficient strategy employs a min-heap architecture, that is comparable to Dijkstra's technique. That's because the heaps must be reconfigured every moment the contents were updated, N stages were utilized to contact each meshes element, with each stage being O(log N). That cystic region in which the seeding points generated by MIC of Isophotes curvature is extremely efficiently extracted using this rapid marched approach. This result demonstrates how the tumor is segregated from the periapicals imageusing the FMM depending on grey levels intensity differences in comparison to the seeded sites (Figure 7).

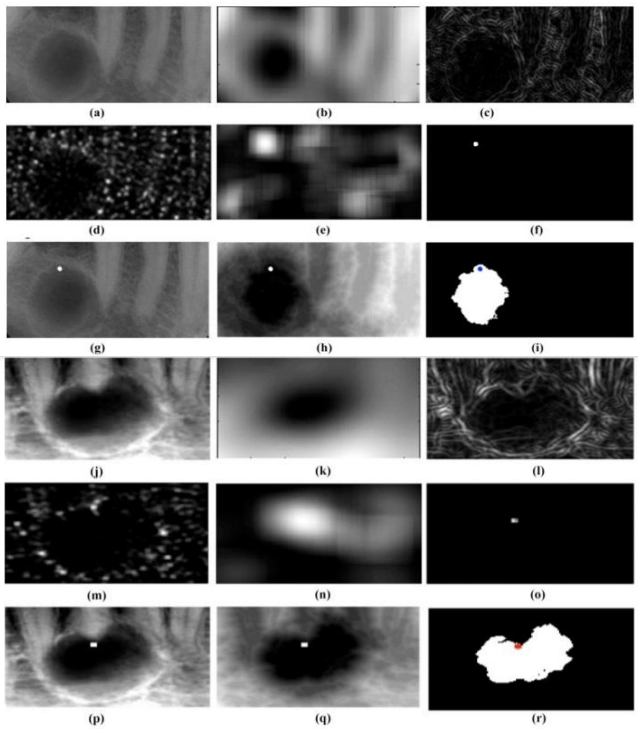

Figure 7. Isophotes curvature, as well as the rapid marches approach, was used to identify an oral tumor

Note: a Source image1, b Gaussian filtering, c curvedness measurement, d isophotes, e transferred imagefollowing blurriness, f maximal IsoCenters, g beginning points determined by MIC, h FMM geodesic length, i tumor recovered by FMM j actual photo 2, k Gaussian fading, l measurement of curvedness, m isophotes, n mapping imagefollowing blurriness, o maximal isocenters, p MIC beginning point, q FMM geodesic length, r FMM retrieved cysts

3.3 Performance evaluation of the proposed method

The modeling of spatial characteristics is more difficult along surfaces than in the imaging planes. Meshes representation is erratic due to the sampling method utilized. In the characterization of the non-Euclidean domains, this is a one-of-a-kind circumstance. Geodesic lengths are the distances among two locations on the surfaces connected by geodesic/lengths minimizing curves.

This dice similarity factor is being used to calculate the overlapping resemblance between the automatic segmentation results as well as the grounds truth and human segments areas AMS & AAS.

$$E = 2|Ams\cap Aas|/|Ams| + |Aas|, where\ |Ams\cap Aas| \quad (16)$$

This overlapped area between the manual segmentation cystic region as well as the segments cystic section using the

proposed approach is represented by $|AMS \cap AAS|$. If indeed the number of the dice coefficients is closer to one, the segmentation result is more similar to the grounds truth image.

4. RESULTS AND DISCUSSION

Maoris Dentals Hospital in Dindigul provided the teeth X-rays images. Figure 8 depicts the example results, with (a)–(i) displaying the intermediary findings for sampling image1 with (j)–(r) displaying the sampling image 2 outcome. The suggested 2-stage, hybrids, automatic approach harvest cysts of any sizes and locations, primarily radicular and follicular cysts, in any place. This suggested approach also retrieved the irregular border without any need for human interference. That tumor area is extracted from the complicated structures of oral X-rays based on the cyst's uneven distribution. Its average runtime for 3 images was determined using the suggested methodology and alternative segmentations technique, as shown in Table 2. Table 3 provides the performances metrics results, which demonstrate that the suggested technique is quicker than that of the other techniques.

In Figure 8, the livewires segmentation is used as the incoming picture's underlying data. The suggested methodology is compared against multilayer histograms-based cutoffs, watersheds, & actively contour approach. Through the livewires, the dentists confirmed the retrieved outcomes of manual cropping. It does, though, necessitate the use of highly skilled medical personnel or manual operators. This Watersheds method produces an under a classification that is over-segmentations, whereas multilayered cutoffs require the amount of the cutoff for classification. Inactivated contours-based classification must be specified as the starting settings. Especially comparts to existing approaches, the suggested technique is reliable for all tumor images and does not need excessive classification. Excluding the identification of the area of interest, there is no requirement for parameter estimation, the choice of several limitations, or human interaction. That sophisticated approach may be used to view periapical & bitewing tooth X-rays images. This graph's geodesic is the smallest path between 2 vertices in graphs, and it connects the edges the quickest. That overlapping zone between the suggested technique's outcome as well as the grounds-truth.

These performances metrics for 3 example photos were generated & presented in Table 3. Average execution time is one of the criteria. Its retrieved cystic region's DICE similarity index, average immediate variation, correctness, & median the measurements demonstrate that the technique is quicker than others, with a median dice factor of 0.89, and that the cystic areas retrieved by a health professional as well as the cystic sections divided by the suggested methods have a significant connection. The highest level of segmentation accuracy attained was 95%.

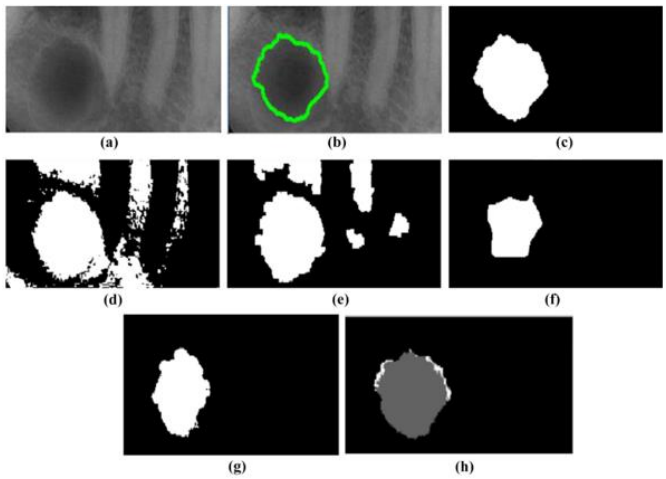

Figure 8. Comparison of the proposed method with other methods

Note: a original image, b live-wire drew, c extracted cyst region by live-wire (ground truth), d multi-level thresholding, e watershed output, f active contour output, g the result of the proposed approach, and h dice similarity calculation

Table 2. Proposed method run time

Image	(C, R)	Size	Mean Run time Automatic seed selection(sec)
Image1	59,99	112X223	3.37
Image2	28,22	164X139	2.56
Image3	69,49	119X143	3.01

Table 3. The performance indicators

Method	Mean time			DICE similarity index			MAD			Accuracy			Cystic region
	P1	P2	P3	P1	P2	P3	P1	P2	P3	P1	P2	P3	
1	54.03	43.55	46.55		GT		8.76	8.34	8.66		GT		65.55
2	9.55	9.67	7.55	0.77	0.53	0.87	8.99	8.66	8.34	0.87	0.84	0.85	71.56
3	3.43	2.34	2.65	0.54	0.88	0.55	9.80	9.67	9.65	0.99	0.99	0.89	71.23
4	8.00	6.34	6.44	0.88	0.76	0.54	8.01	7.54	8.66	0.96	0.78	0.99	61.52
5	3.54	2.55	2.43	0.98	0.54	0.99	5.66	5.55	5.44	0.99	0.77	0.79	65.11

Note: The approach was suggested using (1) Livewires, (2) Multi-level cutoffs, (3) Watersheds algorithm, (4) Actives contour (200 cycles), and (5) suggested technique

5. CONCLUSIONS

Manually segmented or parameters selections for classification are now time-consuming, labor-intensive, as well as demand highly skilled operators. As an outcome, a completely automated image division suited for each situation must be developed to produce an accurate and relevant outcome in therapeutic diagnostics. To divide the tumor in oral X-rays images, the suggested approach incorporated 2 steps, one hybrid, rapid, and automatic. Combining features-based

Isophotes bending & prototype FMM would be used in this hybrid's technique. It detects the cystic region from of the complicated designs of the tooth, the features-based Isophote bending retrieved the largest IsoCenters from the 'inputs cystic picture. This MIC was utilized as a starting point for the technique of rapid marches. For image segments, the FMM is a revised form of the shortest route method. Although the cysts are in an irregular form, the suggested hybrids approach removes them quite effectively. That hybrids technique is effective in segmenting cysts of various sizes & locations. As a result, this procedure is completely automated, quick, as well as effective. Overall examination of findings demonstrates that our hybrids strategy outperforms alternative techniques however no over-segmentations exist. Only the cystic area is precisely excised, with clearly defined borders. Such automated tumor border removal would aid clinicians in subsequent treatment such as tumor seriousness measurement and tumor operation. (1) There is a firm line of demarcation among the cystic region as well as other regions of the tooth, which is achieved by the proposed approach. (2) It is automated; thus, no parameters setup is required. (3) Also, it removes the difficult cystic area (4) It removes every cystic, regardless of size. That technology overcomes the drawbacks of manual segmentation, which is time-intensive, as well as the necessity for qualified radiologists.

REFERENCES

[1] Yang, H., Jo, E., Kim, H.J., et al. (2020). Deep learning for automated detection of cyst and tumors of the jaw in panoramic radiographs. Journal of Clinical Medicine, 9(6): 1839. https://doi.org/10.3390/jcm9061839

[2] Corbella, S., Srinivas, S., Cabitza, F. (2021). Applications of deep learning in dentistry. Oral Surgery, Oral Medicine, Oral Pathology and Oral Radiology, 132(2): 225-238. https://doi.org/10.1016/j.oooo.2020.11.003

[3] Karim, E.T., He, M., Salhoumi, A., Zhigilei, L.V., Galenko, P.K. (2021). Kinetics of solid–liquid interface motion in molecular dynamics and phase-field models: crystallization of chromium and silicon. Philosophical Transactions of the Royal Society A, 379(2205): 20200320. https://doi.org/10.1098/rsta.2020.0320

[4] Latchoumi, T.P., Balamurugan, K., Dinesh, K., Ezhilarasi, T.P. (2019). Particle swarm optimization approach for waterjet cavitation peening. Measurement, 141: 184-189. https://doi.org/10.1016/j.measurement.2019.04.040

[5] Niu, H., Yang, D.L., Sun, Q., Pu, Y., Gao, T., Wang, J.X. (2020). A new method for predicting the maximum filler loading of dental resin composites based on DEM simulations and experiments. Dental Materials, 36(12): e375-e385. https://doi.org/10.1016/j.dental.2020.09.005

[6] Salmanli, M., Yilmaz, G.T., Tuzuner, T. (2021). Investigation of the antimicrobial activities of various antimicrobial agents on Streptococcus mutans Sortase A through computer-aided drug design (CADD) approaches. Computer Methods and Programs in Biomedicine, 212: 106454. https://doi.org/10.1016/j.cmpb.2021.106454

[7] Shan, T., Tay, F.R., Gu, L. (2021). Application of artificial intelligence in dentistry. Journal of Dental Research, 100(3): 232-244. https://doi.org/10.1177%2F0022034520969115

[8] Verma, D., Dong, Y., Sharma, M., Chaudhary, A.K. (2021). Advanced processing of 3D printed biocomposite materials using artificial intelligence. Materials and Manufacturing Processes. https://doi.org/10.1080/10426914.2021.1945090

[9] Sodata, P., Peerapattana, J. (2020). Application of near infrared spectroscopy with chemometrics for qualitative and quantitative dental caries assessment. Vibrational Spectroscopy, 111: 103170. https://doi.org/10.1016/j.vibspec.2020.103170

[10] Meerbeek, B.V., Yoshihara, K., Van Landuyt, K., Yoshida, Y., Peumans, M. (2020). From buonocore's pioneering acid-etch technique to self-adhering restoratives. A status perspective of rapidly advancing dental adhesive technology. Journal of Adhesive Dentistry, 22(1): 7-34. https://doi.org/10.3290/j.jad.a43994

[11] Alhummayani, F.M., Mustafa, Z.A. (2021). A new guide using CBCT to identify the severity of maxillary canine impaction and predict the best method of intervention. Journal of Orthodontic Science, 10(3): 34084759. https://dx.doi.org/10.4103%2Fjos.JOS_41_20

[12] Wang, Q., Geng, P. (2022). Fatigue life prediction method of face-centered cubic single-crystal metals under multiaxial nonproportional loading based on structural mechanical model. Fatigue & Fracture of Engineering Materials & Structures, 45(1): 133-158. https://doi.org/10.1111/ffe.13590

[13] Latchoumi, T.P., Reddy, M.S., Balamurugan, K. (2020). Applied machine learning predictive analytics to SQL injection attack detection and prevention. European Journal of Molecular & Clinical Medicine, 7(2): 3543-3553.

[14] Xu, X., Awad, A., Robles-Martinez, P., Gaisford, S., Goyanes, A., Basit, A.W. (2021). Vat photopolymerization 3D printing for advanced drug delivery and medical device applications. Journal of Controlled Release, 329: 743-757. https://doi.org/10.1016/j.jconrel.2020.10.008

[15] Sivasundaram, S., Pandian, C. (2021). Performance analysis of classification and segmentation of cysts in panoramic dental images using convolutional neural network architecture. International Journal of Imaging Systems and Technology, 31(4): 2214-2225. https://doi.org/10.1002/ima.22625

[16] Miracle, D.B., Li, M., Zhang, Z., Mishra, R., Flores, K.M. (2021). Emerging capabilities for the high-throughput characterization of structural materials. Annual Review of Materials Research, 51: 131-164. https://doi.org/10.1146/annurev-matsci-080619-022100

[17] Polonsky, A.T., Raghavan, N., Echlin, M.P., Kirka, M.M., Dehoff, R.R., Pollock, T.M. (2020). 3D characterization of the columnar-to-equiaxed transition in additively manufactured Inconel 718. Superalloys 2020, pp. 990-1002. https://doi.org/10.1007/978-3-030-51834-9_97

[18] Kwaria, R.J., Mondarte, E.A.Q., Tahara, H., Chang, R., Hayashi, T. (2020). Data-driven prediction of protein adsorption on self-assembled monolayers toward material screening and design. ACS Biomaterials Science & Engineering, 6(9): 4949-4956. https://doi.org/10.1021/acsbiomaterials.0c01008

[19] Grohe, B., Mittler, S. (2021). Advanced non-fluoride

approaches to dental enamel remineralization: The next level in enamel repair management. Biomaterials and Biosystems, 4: 100029. https://doi.org/10.1016/j.bbiosy.2021.100029
[20] Nazarahari, A., Canadinc, D. (2021). Prediction of the NiTi shape memory alloy composition with the best corrosion resistance for dental applications utilizing artificial intelligence. Materials Chemistry and Physics, 258: 123974. https://doi.org/10.1016/j.matchemphys.2020.123974
[21] Leite, A.F., Vasconcelos, K.D.F., Willems, H., Jacobs, R. (2020). Radiomics and machine learning in oral healthcare. PROTEOMICS–Clinical Applications, 14(3): 1900040. https://doi.org/10.1002/prca.201900040
[22] Ren, R., Luo, H., Su, C., Yao, Y., Liao, W. (2021). Machine learning in dental, oral and craniofacial imaging: a review of recent progress. PeerJ, 9: e11451. https://doi.org/10.7717/peerj.11451
[23] Wang, Z., Zhang, J., Xu, Z., et al. (2020). Crystal anisotropy-dependent shear angle variation in orthogonal cutting of single crystalline copper. Precision Engineering, 63: 41-48. https://doi.org/10.1016/j.precisioneng.2020.01.006
[24] Liu, C., Eser, A., Albrecht, T., Stournari, V., Felder, M., Heintze, S., Broeckmann, C. (2021). Strength characterization and lifetime prediction of dental ceramic materials. Dental Materials, 37(1): 94-105. https://doi.org/10.1016/j.dental.2020.10.015
[25] Dong, H., Butler, K.T., Matras, D., et al. (2021). A deep convolutional neural network for real-time full profile analysis of big powder diffraction data. npj Computational Materials, 7(1): 1-9. https://doi.org/10.1038/s41524-021-00542-4
[26] Nagendrababu, V., Aminoshariae, A., Kulild, J. (2021). Artificial intelligence in endodontics: Current applications and future directions. Journal of Endodontics, 47(9): 1352-1357. https://doi.org/10.1016/j.joen.2021.06.003
[27] Wang, X.X., Cao, W.Q., Cao, M.S., Yuan, J. (2020). Assembling nano–microarchitecture for electromagnetic absorbers and smart devices. Advanced Materials, 32(36): 2002112. https://doi.org/10.1002/adma.202002112
[28] Bandela, V., Kanaparthi, S. (2020). Finite Element Analysis and Its Applications in Dentistry. In Finite Element Methods and Their Applications. London, UK: IntechOpen.
[29] Putra, R.H., Doi, C., Yoda, N., Astuti, E.R., Sasaki, K. (2022). Current applications and development of artificial intelligence for digital dental radiography. Dentomaxillofacial Radiology, 51(1): 20210197. https://doi.org/10.1259/dmfr.20210197